

Negative parity baryons in quenched anisotropic lattice QCD

Y. Nemoto*,¹ N. Nakajima,² H. Matsufuru,¹ and H. Suganuma³

¹*Yukawa Institute for Theoretical Physics, Kyoto University, Kyoto 606-8502, Japan*

²*Center of Medical Information Science, Kochi Medical School, Kochi, 783-8505 Japan*

³*Faculty of Science, Tokyo Institute of Technology, Tokyo 152-8551, Japan*

(Dated: May 22, 2019)

We investigate the negative parity baryon spectrum in quenched lattice QCD. We employ the anisotropic lattice with standard Wilson gauge and $O(a)$ improved Wilson quark actions at three values of lattice spacings with renormalized anisotropy $\xi = a_\sigma/a_\tau = 4$, where a_σ and a_τ are spatial and temporal lattice spacings. The negative parity baryons are measured as the parity partner of the ground state baryons, i.e., by the same correlation functions as the positive parity baryons. In relation to $\Lambda(1405)$, we pay much attention to the $SU(3)$ flavor singlet negative parity baryon, which is described as a three-quark state in quenched lattice QCD. For the flavor octet and decuplet negative parity baryons, the calculated masses are close to the experimental values of corresponding lowest-lying negative parity baryons. In contrast the flavor singlet baryon is much heavier than $\Lambda(1405)$, which indicates that the $\Lambda(1405)$ would be a multi-quark state such as the $N\bar{K}$ molecule rather than the flavor singlet three-quark state.

PACS numbers: 12.38.Gc, 14.20.Gk, 14.20.Jn

I. INTRODUCTION

The lattice QCD simulation has become a powerful method to investigate hadron properties directly based on QCD. The spectroscopy of lowest-lying hadrons in the quenched approximation, i.e. without the dynamical quark effect, has been almost established, and reproduces their experimental values within 10 % deviations [1]. Extensive simulations including dynamical quarks are in progress and would give us detailed understanding of the spectra of these ground state hadrons [2]. In contrast, calculations of excited state hadrons are far from established, even at the quenched level. In this paper, we focus on the low-lying negative parity baryon spectrum, in particular the nature of the flavor singlet state, $\Lambda(1405)$. $\Lambda(1405)$ is the most mysterious baryon from the viewpoint of the quark model: it is the lightest negative parity baryon, while it contains strangeness. The primary goal of this paper is to clarify whether a naive three-quark (3Q) picture can explain the mass of $\Lambda(1405)$ using quenched lattice QCD. Since detailed lattice studies of the negative-parity baryons have been started rather recently [3, 4, 5, 6, 7, 8, 9], it is important to calculate their masses to establish the spectra at the quenched level, as well as the foundation to understand the peculiar nature of $\Lambda(1405)$.

Excited state baryons have been so far mainly investigated within the framework of the nonrelativistic quark model, in which baryons can be classified by the spin-flavor $SU(6)$ symmetry. While the ground state baryons have completely symmetric spin-flavor wave functions and form the 56-dimensional representation, the low-

lying negative parity baryons are parts of the $L = 1$ orbitally excited states and belong to the $SU(6)$ 70-dimensional representation. We summarize the classification of the $SU(6)$ symmetry and its assignment to experimental baryon masses in Table I. Both the non-relativistic [10] and semirelativistic [11] quark models reproduce the negative parity baryon spectrum fairly well in the octet and decuplet sectors [12]. Such success of the quark models implies that the constituent quark picture well holds and the gluonic excitation modes play a less important role. Recent results of lattice QCD calculations of the static three quark potential are in accordance with the adopted forms in these potential model approaches [13, 14, 15]. Furthermore, large excitation energy of the flux-tube vibration modes observed in lattice QCD simulation explains why the potential models without such excitations well describe the hadron spectra [16].

Among the low-lying negative parity baryons, $\Lambda(1405)$ is an exception of such success of the potential models. In fact it is much lighter than the lowest-lying non-strange negative parity baryons, $N(1520)$ with $J^P = 3/2^-$ and $N(1535)$ with $J^P = 1/2^-$. There are two representations proposed for $\Lambda(1405)$: an $SU(3)$ flavor singlet 3Q state, and an $N\bar{K}$ bound state (five-quark (5Q) system). The naive quark model is based on the former picture, which predicts that the $\Lambda(1405)$ and $\Lambda(1520)$ with $J^P = 3/2^-$ are nearly degenerate [10, 11]. Although the difference between them is attributed to the LS -force, such a strong LS splitting is not observed in other baryon spectra. To reproduce the mass of $\Lambda(1405)$ within the naive quark model picture, we therefore need another mechanism. The other picture, the $N\bar{K}$ bound state like a hadronic molecule is an interesting interpretation, because $\Lambda(1405)$ lies about 30 MeV below the $\bar{K}N$ threshold. The binding energy of 30 MeV is very large compared with, say, that of the deuteron, about

*Present address: RIKEN BNL Research Center, BNL, Upton, NY 11973

2.2 MeV. If this picture actually holds true, studies of such an exotic hadronic state would also be important for understanding of the manifestation of strangeness in the hyper-nuclei and the neutron stars.

The 3Q and the 5Q states, however, would mix in the real world. Therefore, a more realistic question is: which is the dominant component of the $\Lambda(1405)$, the 3Q state or 5Q state? We challenge this question using lattice QCD simulation. In lattice QCD simulation, even if one chooses the operator as 3Q or 5Q state, it generally overlaps with both the states through the dynamical quark loop effect. In the quenched simulation, however, such an effect is absent, and hence the properties of genuine 3Q and 5Q states can be singled out. In this paper, we focus on the 3Q state and investigate whether this picture can explain the mass of $\Lambda(1405)$. Apparent discrepancy with the experimentally observed mass implies that the 5Q state gives significant contribution to the physical $\Lambda(1405)$ state. Direct calculations of the 5Q and mixed states are future subjects. In practice, lattice QCD results suffer from various systematic errors. It is therefore essential to compare the mass of the flavor singlet 3Q state with other negative parity baryon masses as well as with lowest-lying baryon masses.

It is also important to understand the gross structure of low-lying negative parity baryon spectrum in relation to the spontaneous chiral symmetry breaking of QCD. If the chiral symmetry is restored, such as at high temperature and/or density, the masses of a baryon and its parity partner should be degenerate. The spontaneous chiral symmetry breaking causes mass splitting between positive and negative parity baryons. It is important to study nonperturbatively negative parity baryons in terms of the parity partners of the positive parity ones. Although the present lattice formulation breaks the chiral symmetry explicitly, the effect of the broken symmetry can be investigated by the extrapolation to the limit of massless quarks. This is an advantage of lattice QCD over, *e.g.*, naive quark models which do not incorporate the chiral symmetry.

The masses of the negative parity baryons as the parity partner of the positive parity ones can be extracted from the same correlators as for the latter but in the opposite Euclidean time direction. One problem in extracting the former lies in the rapid growth of the statistical fluctuations in the correlation functions, which makes it difficult to identify the reliable range of Euclidean temporal distance where the relevant information is extracted. We adopt the anisotropic lattice, on which the temporal lattice spacing a_τ is finer than the spatial one, a_σ [18]. High resolution in the temporal direction makes us easy to follow the change of correlators, and hence to identify the relevant range for extraction of masses. This approach may equally efficient for the correlators of heavy particles, such as the glueballs, for which the noises grow rapidly against the signals. In this work, we adopt the standard Wilson plaquette gauge action and $O(a)$ improved Wilson quark action, for which the sizes of errors are rather

well evaluated [19, 20]. The simulations are performed on the same lattices as in Ref. [20], the quenched anisotropic lattices with renormalized anisotropy $\xi = a_\sigma/a_\tau = 4$ at three lattice spacings in the range of $a_\sigma^{-1} \simeq 1\text{--}2$ GeV. Ref. [20] tuned the quark parameters and computed the light hadron spectrum to discuss effects of uncertainties due to anisotropy on the spectrum. We here extend their analysis to the negative parity baryons and discuss physical implications of the results.

This paper is organized as follows. In Section II, we summarize the anisotropic lattice actions used in this work. Section III describes the numerical simulations and their results, whose physical consequences are discussed in Section IV. The last section is dedicated to our conclusion and perspective for further studies. Our preliminary results have been reported in Ref. [3].

II. ANISOTROPIC LATTICE

We employ the standard Wilson plaquette gauge action and the $O(a)$ improved Wilson quark action on anisotropic lattices, because for these actions there are available results of calibration which control the systematic uncertainties to the sufficient level for the present purpose [19, 20]. We carry out the numerical simulations on the same lattices as in Ref. [20]. To make this paper self-contained, we here briefly summarize the anisotropic lattice actions. The parameters used in our numerical simulation are described in the next section.

The gauge field action is in the form

$$S_G = \beta \sum_x \left\{ \sum_{i>j=1}^3 \frac{1}{\gamma_G} \left[1 - \frac{1}{3} \text{ReTr} U_{ij}(x) \right] + \sum_{i=1}^3 \gamma_G \left[1 - \frac{1}{3} \text{ReTr} U_{i4}(x) \right] \right\}, \quad (1)$$

where β is the coupling and $U_{\mu\nu}$ denotes the parallel transport around a plaquette in μ - ν plane,

$$U_{\mu\nu}(x) = U_\mu(x) U_\nu(x + \hat{\mu}) U_\mu^\dagger(x + \hat{\nu}) U_\nu^\dagger(x) \quad (2)$$

The gluon field is represented with the link variable as $U_\mu \simeq \exp(-iga_\mu A_\mu)$. The bare anisotropy γ_G coincides with the renormalized anisotropy $\xi = a_\sigma/a_\tau$ at the tree level. In a practical case, the bare anisotropy is no longer the same as ξ due to the quantum effect, and one needs to measure ξ through some observables for each input value of γ_G . Although ξ is in general a function of gauge and quark parameters, (β, γ_G) and (κ, γ_F) , on a quenched lattice the calibrations of the gauge and quark actions can be performed separately. For the gauge action of the form (1), Klassen nonperturbatively obtained an expression of γ_G in terms of β and ξ with 1% accuracy using the Wilson loops [19]. We make use of his result in this work.

For the Wilson type quark action, $O(a)$ improvement is significant in quantitative computation of hadron spectrum. Among several types of the anisotropic lattice

TABLE I: Quark model assignments for experimentally observed baryons in terms of a spin-flavor SU(6) basis[17].

$SU(6)$ rep.	$SU(3)_f$ rep.	J^P	$S = 0$	$S = -1, I = 0$	$S = -1, I = 1$	$S = -2$	$S = -3$
56 ($L = 0$)	2_8	$\frac{1}{2}^+$	$N(939)$	$\Lambda(1116)$	$\Sigma(1193)$	$\Xi(1318)$	
	$^4_{10}$	$\frac{3}{2}^+$	$\Delta(1232)$		$\Sigma(1385)$	$\Xi(1530)$	$\Omega(1672)$
70 ($L = 1$)	2_8	$\frac{1}{2}^-$	$N(1535)$	$\Lambda(1670)$	$\Sigma(1620)$	$\Xi(?)$	
		$\frac{3}{2}^-$	$N(1520)$	$\Lambda(1690)$	$\Sigma(1670)$	$\Xi(1820)$	
		$\frac{5}{2}^-$	$N(1650)$	$\Lambda(1800)$	$\Sigma(1750)$	$\Xi(?)$	
	4_8	$\frac{1}{2}^-$	$N(1700)$	$\Lambda(?)$	$\Sigma(?)$	$\Xi(?)$	
		$\frac{3}{2}^-$	$N(1700)$	$\Lambda(?)$	$\Sigma(?)$	$\Xi(?)$	
		$\frac{5}{2}^-$	$N(1675)$	$\Lambda(1830)$	$\Sigma(1775)$	$\Xi(?)$	
		$\frac{7}{2}^-$	$\Delta(1620)$		$\Sigma(?)$	$\Xi(?)$	$\Omega(?)$
	$^2_{10}$	$\frac{1}{2}^-$	$\Delta(1700)$		$\Sigma(?)$	$\Xi(?)$	$\Omega(?)$
		$\frac{3}{2}^-$					
		$\frac{5}{2}^-$					
	2_1	$\frac{1}{2}^-$		$\Lambda(1405)$			
		$\frac{3}{2}^-$		$\Lambda(1520)$			

quark action, we use the form proposed in Refs. [20, 21, 22]. This is because in this form the calibration with a good precision is rather easy in the light quark mass region, since the quark mass dependence is expected to be small there, as was numerically shown in Ref. [20].

The quark action is written as

$$S_F = \sum_{x,y} \bar{\psi}(x) K(x,y) \psi(y), \quad (3)$$

$$\begin{aligned}
K(x,y) = & \delta_{x,y} \\
& -\kappa_\tau \left\{ (1-\gamma_4) U_4(x) \delta_{x+\hat{4},y} + (1+\gamma_4) U_4^\dagger(x-\hat{4}) \delta_{x-\hat{4},y} \right\} \\
& -\kappa_\sigma \sum_i \left\{ (r-\gamma_i) U_i(x) \delta_{x+\hat{i},y} + (r+\gamma_i) U_i^\dagger(x-\hat{i}) \delta_{x-\hat{i},y} \right\} \\
& -\kappa_\sigma c_E \sum_i \sigma_{i4} F_{i4} \delta_{x,y} - r \kappa_\sigma c_B \sum_{i>j} \sigma_{ij} F_{ij} \delta_{x,y}, \quad (4)
\end{aligned}$$

where ψ denotes the anticommuting quark field, κ_σ and κ_τ are the spatial and temporal hopping parameters, r is the spatial Wilson parameter and c_E , c_B are the clover coefficients. In principle for a given κ_σ , the four parameters $\kappa_\sigma/\kappa_\tau$, r , c_E and c_B should be tuned so that Lorentz symmetry is satisfied up to discretization errors of $O(a^2)$. Following Refs. [20, 21, 22], we set the spatial Wilson parameter as $r = 1/\xi$ and the clover coefficients as the tadpole-improved tree-level values, namely,

$$r = 1/\xi, \quad c_E = 1/u_\sigma u_\tau^2, \quad c_B = 1/u_\sigma^3. \quad (5)$$

To reduce large contribution from the tadpole diagram, the tadpole improvement [24] is applied by rescaling the link variables as $U_i(x) \rightarrow U_i(x)/u_\sigma$ and $U_4(x) \rightarrow U_4(x)/u_\tau$, with the mean-field values of the spatial and temporal link variables, u_σ and u_τ , respectively. This is equivalent to redefining the hopping parameters with the tadpole-improved ones (with tilde) through $\kappa_\sigma = \tilde{\kappa}_\sigma/u_\sigma$ and $\kappa_\tau = \tilde{\kappa}_\tau/u_\tau$. We define the anisotropy parameter γ_F as $\gamma_F \equiv \tilde{\kappa}_\tau/\tilde{\kappa}_\sigma$. This is the parameter of action to be tuned nonperturbatively in the numerical simulation. It

is convenient to define κ as

$$\frac{1}{\kappa} \equiv \frac{1}{\tilde{\kappa}_\sigma} - 2(\gamma_F + 3r - 4) = 2(m_0 \gamma_F + 4), \quad (6)$$

where m_0 is the bare quark mass in temporal lattice units. This κ plays the same role as in the case of isotropic lattice, and is convenient to parameterize a quark mass together with the bare anisotropy γ_F .

The above action is constructed following the Fermilab approach [20], which proposes to tune the bare anisotropy parameter so that the rest and kinetic masses equal each other. In practice, hadronic states are convenient to carry out this program. In Ref. [20], the bare anisotropy was tuned nonperturbatively using the relativistic dispersion relation of the pseudoscalar and vector mesons. The main result of Ref. [20] is as follows: They tuned γ_F in the quark mass range from the strange to charm quark masses with 1% statistical accuracy, and found that the tuned bare anisotropy, γ_F^* , is well fitted to the linear form in m_q^2 , where $m_q = (\kappa^{-1} - \kappa_c^{-1})/2\xi$ is naively defined quark mass. Then γ_F^* in the massless limit was obtained with 2% accuracy, 1% of statistical error and 1% of systematic error in the form of fit in terms of m_q . Then they computed the light hadron spectrum using the value of γ_F^* at the chiral limit, and observed the effect of uncertainty in γ_F^* on the spectrum for physical quark masses at the level of 1%. In the present study, we also treat the same quark mass region and therefore adopt the value of γ_F^* in the chiral limit. The precision of 2% error in γ_F^* is sufficient for present purpose.

As was pointed out in Refs. [20, 21], with the choice $r = 1/\xi$, the action (4) leads to a smaller spatial Wilson term for a larger anisotropy ξ . Since the negative parity baryons measured in this paper are the ground state of the parity projected baryon correlators, the statements in Ref. [20] for light hadrons also hold in our calculation. Our coarsest lattice has the cutoff $a_\tau^{-1} \simeq 4.0$ GeV, and seems sufficiently large to avoid the naive excited state contamination due to the doublers in the ground state signals, while more nontrivial doubler effect such as the

shift of energy through the mixing of the ground states and the doubler states is not excluded. $a_\tau^{-1} \simeq 8$ GeV of our finest lattice would be sufficiently large to avoid the doubler effect.

III. NUMERICAL SIMULATION

A. Lattice Setup

The numerical simulation is performed on the same lattices as in Ref. [20]. Here we briefly summarize the fundamental parameters and physical quantities. We use the three anisotropic lattices with the renormalized anisotropy $\xi = 4$, at the quenched level. The statistical uncertainties are, otherwise noted, estimated by the Jackknife method with appropriate binning.

The lattice sizes and parameters in generating the gauge field configurations are listed in Table II. The spatial lattice scales roughly cover 1–2 GeV. The values of bare gluonic anisotropy, γ_G , are chosen according to the result by Klassen [19]. The uncertainty of his expression is of the order of 1%, and in the following analysis we do not include this uncertainty in the quoted statistical errors. The configurations are separated by 2000 (1000) pseudo-heat-bath sweeps, after 20000 (10000) thermalization sweeps at $\beta=5.95$ and 6.10 (5.75). The configurations are fixed to the Coulomb gauge, which is convenient in applying the smearing of hadron operators.

The mean-field values of link variables are determined on the smaller lattices with half size in temporal extent and otherwise with the same parameters for $\beta = 5.75$ and 5.95, while at $\beta = 6.10$ the lattice size is $16^3 \times 64$. The mean-field values, u_σ and u_τ , are obtained as the averages of the link variables in the Landau gauge, where the mean-field values are self-consistently used in the fixing condition [21]. In a study of hadron spectrum, it is convenient to define the lattice scales through a hadronic quantity. We choose to determine a_σ^{-1} through the K^* meson mass, $m_{K^*} = 893.9$ MeV (isospin averaged). The procedure is the same as in Ref. [20], while with larger statistics. The result is quoted in Table II as $a_\sigma^{-1}(m_{K^*})$.

The quark parameters are listed in Table III. These hopping parameters roughly cover the quark masses $m_q \simeq m_s - 2m_s$. The numbers of configurations are larger than those of the hadronic spectroscopy in Ref. [20]. As already noted in the previous section, the values of γ_F and κ_c are taken from the result of Ref. [20]. Although the uncertainty of 2% level is associated with the values of γ_F , the quoted errors of hadron masses in the following analysis do not include this uncertainty. according to Ref. [20], the effect of this uncertainty in the physical masses of vector mesons and positive parity baryons are at most of order of 1%. For the negative parity baryon masses, the effect is expected to be similar amount and not significant compared with the present level of statistical error. Therefore, we do not examine this effect in this paper.

As described later, we first extrapolate the vector meson mass linearly in the pseudoscalar meson mass squared to the point at which the ratio of these meson masses are equal to the physical value, m_{K^*}/m_K . At this point, aforementioned lattice scale is determined. The physical (u, d) and s quark masses are determined through the π and K meson masses, $m_\pi^\pm = 139.6$ MeV and $m_K = 495.7$ MeV (isospin averaged), respectively.

B. Baryon correlators

We measure the correlators in pseudoscalar and vector meson channels and octet (Σ and Λ types), decuplet and singlet channels of SU(3) flavor representation of baryons. As listed in Table IV, we use the standard meson and baryon operators which have the same quantum numbers as the corresponding baryons and survive in the nonrelativistic limit. It is known that there are mainly two ways to choose the baryon operator. One is the operator taken here, $(q^T C \gamma_5 q)q$, and the other is of the form $(q^T C q) \gamma_5 q$. There are two reasons why we take the former. It is well-known that the former operators strongly couple to the the ground state baryons and reproduce experimental values well. Therefore, it is suitable for investigation of the parity partner of the ground state baryons. Furthermore recent lattice calculation shows that these two operators give the similar results for the negative parity baryon spectrum but the latter is more noisy [5].

For baryons, two of three quark masses are taken to be the same value as specified by the hopping parameter κ_1 , and the other quark mass is specified by κ_2 . This corresponds to taking the same value for u, d current quark masses as $m_u = m_d \equiv m_n$. Then, the baryon masses are expressed as the function of two masses m_1 and m_2 , or equivalently of κ_1 and κ_2 , like $m_B(\kappa_1, \kappa_2)$. In the source operator, each quark field is smeared with the Gaussian function of width $\simeq 0.4$ fm.

At large t (and large $N_t - t$), the baryon correlators are represented as

$$\begin{aligned} G_B(t) &\equiv \sum_{\vec{x}} \langle B(\vec{x}, t) \bar{B}(\vec{x}, 0) \rangle \\ &= (1 + \gamma_4) \left[c_{B^+} \cdot e^{-tm_{B^+}} + b c_{B^-} \cdot e^{-(N_t-t)m_{B^-}} \right] \\ &\quad + (1 - \gamma_4) \left[b c_{B^+} \cdot e^{-(N_t-t)m_{B^+}} + c_{B^-} \cdot e^{-tm_{B^-}} \right], \quad (7) \end{aligned}$$

where $b = +1$ and -1 for the periodic and antiperiodic temporal boundary conditions for the quark fields. Since we adopt the standard Dirac representation for γ matrices, the upper and lower two components correspond to the first and second contributions of Eq. (7).

Combining the parity-projected correlators under two boundary conditions, one can single out the positive and negative parity baryon states with corresponding masses m_{B^+} and m_{B^-} , respectively, without contributions from the backward propagating parity partners. In practical

TABLE II: Lattice parameters. The scale $a_\sigma^{-1}(m_{K^*})$ is determined from the K^* meson mass. The mean-field values are defined in the Landau gauge. The statistical uncertainty of u_τ is less than the last digit. The details for these parameters are described in [20].

β	γ_G	size	u_σ	u_τ	$a_\sigma^{-1}(m_{K^*})$ [GeV]
5.75	3.072	$12^3 \times 96$	0.7620(2)	0.9871	1.034(6)
5.95	3.1586	$16^3 \times 128$	0.7917(1)	0.9891	1.499(9)
6.10	3.2108	$20^3 \times 160$	0.8059(1)	0.9901	1.871(14)

TABLE III: Quark parameters. The values of γ_F and κ_c are from Ref. [20].

β	γ_F	κ_c	N_{conf}	values of κ
5.75	3.909	0.12640(5)	400	0.1240, 0.1230, 0.1220, 0.1210
5.95	4.016	0.12592(6)	400	0.1245, 0.1240, 0.1235, 0.1230
6.10	4.034	0.12558(4)	400	0.1245, 0.1240, 0.1235, 0.1230

simulation, however, we take a sufficient temporal extent so that we can observe an enough range of plateau in effective mass plot for extraction of mass in each parity channel, and hence there is no advantage in computing correlators under two boundary conditions except for the reduction of statistical fluctuation. We obtain the baryon correlators at $\beta = 5.75$ under two boundary conditions, and compare the statistical fluctuations in the parity-projected correlator and in not projected one. We conclude that it is not worth doubling the computational cost and hence adopt only the periodic boundary condition hereafter. Instead, at each β we obtain the correlators with the source at $t = N_t/2$ in addition to ones with the source at $t = 0$, and average them. This is efficient to reduce the statistical errors for limited number of configurations.

C. Results

Fig. 1 shows the effective mass plots for the baryon correlators at $\beta = 6.10$. The effective mass is defined without considering the contribution of the associated parity partner propagating backward from the source at $t = N_t$,

$$m_{\text{eff}} = \ln \left(\frac{G_B(t)}{G_B(t+1)} \right). \quad (8)$$

We observe that in the region where the effective mass exhibits a plateau, the contribution of parity partner is sufficiently small. In particular for the negative parity baryon channels, fine temporal lattice spacing seems to be helpful to specify the region in which the ground state dominates.

The meson correlator is fitted to the single hyperbolic cosine form and analyzed independently of Ref. [20]. The results are shown in Fig. 2. and consistent with Ref. [20]. For the baryons, we fit the data to a single exponential form. The result is listed in Tables V, VI and VII.

Following Ref. [20], we extrapolate the hadron masses to the chiral limit in terms of the pseudoscalar meson mass squared, instead of $1/\kappa$. The assumed relation between PS meson mass and quark mass is

$$m_{PS}^2(m_1, m_2) = B \cdot (m_1 + m_2), \quad (9)$$

then for the degenerate quark masses, $m_1 = m_2$, $m_{PS}^2 = 2Bm_1$ holds. Instead of m_i ($i=1,2$), one can extrapolate other hadron masses in term of $m_{PS}(m_i, m_i)^2$ to the chiral limit.

In our calculation for baryons, two of quark masses are taken to be the same value, m_1 , and the other quark mass m_2 is taken to be an independent value. Then, the baryon masses are expressed as the function of m_1 and m_2 like $m_B(m_1, m_2)$, and therefore are to be depicted on the (m_1, m_2) plane. However, the result for the baryon masses seem to be well described with the linear relation,

$$m_B(m_1, m_2, m_3) = m_B(0, 0, 0) + B_B \cdot (2m_1 + m_2). \quad (10)$$

Therefore, we fit the baryon mass data to the linear form in the sum of corresponding PS meson masses squared. Although it is reported that there is the non-analyticity in the chiral extrapolation of the nucleon even in the quenched level[25], we do not argue it here because we do not observe its distinct behavior for both the positive and negative parity baryons. The vector meson is also fitted to a linear function in $m_1 + m_2$.

The results of fits are shown in Fig. 3 for each lattice. The horizontal axis is the averaged pseudoscalar meson mass squared,

$$\langle m_{PS}^2(m_i) \rangle = \frac{1}{N_q} \sum_{i=1}^{N_q} m_{PS}^2(m_i, m_i) = \frac{1}{N_q} \sum_{i=1}^{N_q} 2Bm_i \quad (11)$$

with $N_q = 3$ for baryons. The results of fits are displayed as the solid lines in these figures. The linear relation seems to hold well.

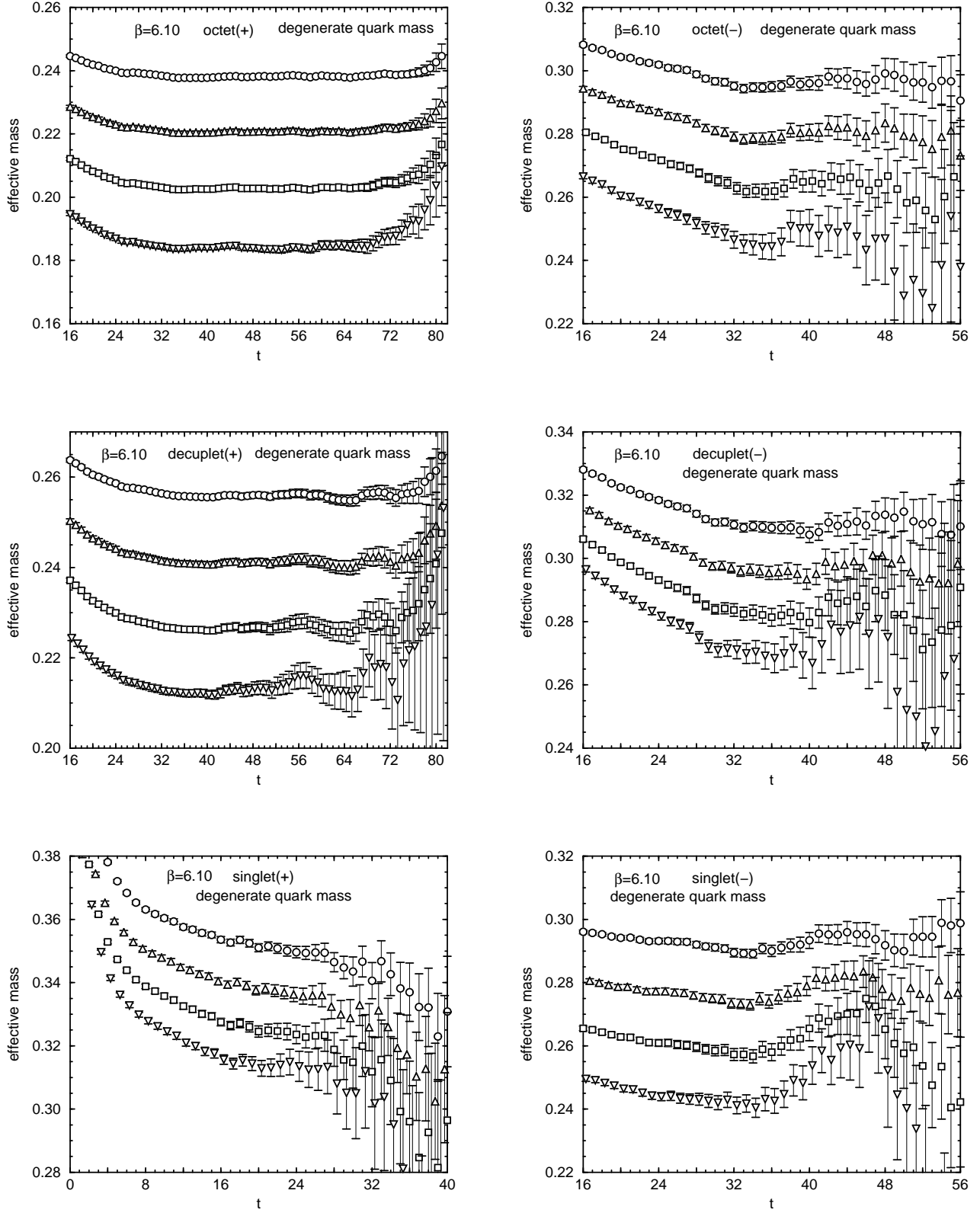


FIG. 1: Effective mass plots for octet, decuplet and singlet baryon correlators with degenerate quark masses at $\beta = 6.10$. The symbols correspond to $\kappa = 0.1230, 0.1235, 0.1240$ and 0.1245 from top to bottom in each figure. The left figures are for the positive parity baryons and the right for the negative parity ones.

TABLE IV: Hadron operators. For baryons, the contraction with the color index is omitted. C denotes the charge conjugate matrix.

Meson	Pseudoscalar	$M(K) = \bar{s}\gamma_5 u$
	Vector	$M_k(K^*) = \bar{s}\gamma_k u$
Baryon	Octet	$B_\alpha(\Sigma^0) = (C\gamma_5)_{\beta\gamma}[u_\alpha(d_\beta s_\gamma - s_\beta d_\gamma) - d_\alpha(s_\beta u_\gamma - u_\beta s_\gamma)]$
	Octet (Λ)	$B_\alpha(\Lambda) = (C\gamma_5)_{\beta\gamma}[u_\alpha(d_\beta s_\gamma - s_\beta d_\gamma) + d_\alpha(s_\beta u_\gamma - u_\beta s_\gamma) - 2s_\alpha(u_\beta d_\gamma - d_\beta u_\gamma)]$
	Singlet	$B_\alpha(\Lambda_1) = (C\gamma_5)_{\beta\gamma}[u_\alpha(d_\beta s_\gamma - s_\beta d_\gamma) + d_\alpha(s_\beta u_\gamma - u_\beta s_\gamma) + s_\alpha(u_\beta d_\gamma - d_\beta u_\gamma)]$
	Decuplet	$B_{\alpha k}(\Sigma^{*0}) = (C\gamma_k)_{\beta\gamma}[u_\alpha(d_\beta s_\gamma + s_\beta d_\gamma) + d_\alpha(s_\beta u_\gamma + u_\beta s_\gamma) + s_\alpha(u_\beta d_\gamma + d_\beta u_\gamma)]$

TABLE V: Baryon spectrum at $\beta = 5.75$ in the temporal lattice unit. Note that when quark masses are degenerate, i.e. $\kappa_1 = \kappa_2$, the Σ -type and the Λ -type octet baryon correlators are identical and hence we omitted the latter.

Positive parity baryons						Negative parity baryons			
κ_1	κ_2	$m_{oct(\Sigma)}$	$m_{oct(\Lambda)}$	m_{sing}	m_{dec}	$m_{oct(\Sigma)}$	$m_{oct(\Lambda)}$	m_{sing}	m_{dec}
0.1210	0.1210	0.4281(9)	—	0.6426(56)	0.4606(16)	0.5443(52)	—	0.5355(30)	0.5630(54)
0.1210	0.1220	0.4171(10)	0.4186(10)	0.6349(59)	0.4518(17)	0.5355(56)	0.5356(57)	0.5265(32)	0.5548(59)
0.1210	0.1230	0.4059(10)	0.4091(10)	0.6267(64)	0.4433(19)	0.5271(61)	0.5270(64)	0.5175(34)	0.5467(66)
0.1210	0.1240	0.3946(11)	0.3998(11)	0.6184(69)	0.4352(21)	0.5189(68)	0.5178(78)	0.5089(37)	0.5386(78)
0.1220	0.1210	0.4083(10)	0.4066(10)	0.6275(63)	0.4430(19)	0.5269(61)	0.5269(60)	0.5173(33)	0.5465(65)
0.1220	0.1220	0.3970(11)	—	0.6206(68)	0.4341(20)	0.5181(66)	—	0.5080(35)	0.5382(71)
0.1220	0.1230	0.3855(11)	0.3874(11)	0.6132(74)	0.4256(22)	0.5095(73)	0.5091(75)	0.4989(38)	0.5300(79)
0.1220	0.1240	0.3737(12)	0.3780(12)	0.6055(81)	0.4176(25)	0.5012(82)	0.4994(90)	0.4899(41)	0.5217(93)
0.1230	0.1210	0.3885(11)	0.3845(11)	0.6116(74)	0.4259(22)	0.5091(77)	0.5099(74)	0.4990(38)	0.5302(81)
0.1230	0.1220	0.3769(12)	0.3747(12)	0.6063(81)	0.4171(24)	0.5001(83)	0.5008(81)	0.4895(41)	0.5218(89)
0.1230	0.1230	0.3650(12)	—	0.6004(89)	0.4085(27)	0.4913(92)	—	0.4801(44)	0.513(10)
0.1230	0.1240	0.3527(13)	0.3554(13)	0.5939(99)	0.4004(32)	0.483(11)	0.481(11)	0.4707(48)	0.505(12)
0.1240	0.1210	0.3689(13)	0.3612(13)	0.5936(89)	0.4099(30)	0.489(11)	0.4928(98)	0.4805(46)	0.514(11)
0.1240	0.1220	0.3569(14)	0.3512(14)	0.591(10)	0.4010(33)	0.480(12)	0.483(11)	0.4708(49)	0.505(12)
0.1240	0.1230	0.3445(15)	0.3414(15)	0.588(11)	0.3922(37)	0.470(13)	0.473(12)	0.4610(53)	0.496(14)
0.1240	0.1240	0.3317(16)	—	0.585(13)	0.3838(45)	0.460(15)	—	0.4509(58)	0.486(16)
fit range		24–40	24–40	12–20	28–40	20–32	20–32	16–24	20–32

As stated in Section III, we determine the scale a_τ^{-1} through the K^* meson mass. The physical (u , d) and s quark masses are determined with the π and K meson masses. The scale of the vertical and horizontal axes in Fig. 3 are set in this way. The corresponding hadron masses for the physical quark masses are listed in Table VIII. These results for the meson masses and positive parity baryon masses are consistent with those obtained in Ref. [20] with smaller statistics.

D. Systematic errors

Finally before discussing physical implications of our numerical results, we briefly comment on the sources of systematic uncertainties.

- *Anisotropy (calibration)*

According to the detailed inspection given in [20], the 2% uncertainty in γ_F causes uncertainties in

hadron masses at 1% level. Although the effect of uncertainty coming from anisotropy on the negative parity baryon masses is unknown, its size is expected to be the same level as for the positive parity baryons and smaller than their statistical errors. Therefore, we do not perform a detailed analysis of the calibration uncertainty here. The uncertainty in γ_G , the gluonic anisotropy parameter, is also kept within 1% level, and hence for the same reason as for γ_F , we do not argue its effect on the negative parity baryon masses.

- *Finite volume effects*

Since the excited baryons may have larger spatial extent than the ground state baryons, they may seriously suffer from the finite size effects. Our present three lattices, however, have almost the same size (~ 2 fm), and we cannot examine the finite volume effects on these lattices. In Ref. [6], the finite volume effect on the negative

TABLE VI: The same as Table V for $\beta = 5.95$.

κ_1	κ_2	Positive parity baryons				Negative parity baryons			
		$m_{oct}(\Sigma)$	$m_{oct}(\Lambda)$	m_{sing}	m_{dec}	$m_{oct}(\Sigma)$	$m_{oct}(\Lambda)$	m_{sing}	m_{dec}
0.1230	0.1230	0.2785(7)	–	0.4279(27)	0.3041(10)	0.3537(28)	–	0.3460(32)	0.3771(36)
0.1230	0.1235	0.2722(7)	0.2732(7)	0.4240(28)	0.2993(10)	0.3482(30)	0.3487(30)	0.3407(33)	0.3728(39)
0.1230	0.1240	0.2658(7)	0.2680(8)	0.4202(30)	0.2945(11)	0.3428(32)	0.3441(34)	0.3355(36)	0.3690(43)
0.1230	0.1245	0.2592(8)	0.2628(8)	0.4165(34)	0.2899(12)	0.3374(35)	0.3406(40)	0.3306(40)	0.3661(48)
0.1235	0.1230	0.2675(7)	0.2664(7)	0.4203(30)	0.2944(11)	0.3434(33)	0.3430(32)	0.3354(35)	0.3686(42)
0.1235	0.1235	0.2610(8)	–	0.4168(33)	0.2896(12)	0.3378(35)	–	0.3299(38)	0.3643(45)
0.1235	0.1240	0.2545(8)	0.2557(8)	0.4133(36)	0.2848(12)	0.3322(38)	0.3330(39)	0.3246(41)	0.3604(49)
0.1235	0.1245	0.2477(8)	0.2504(9)	0.4099(40)	0.2801(14)	0.3268(42)	0.3291(46)	0.3195(45)	0.3575(56)
0.1240	0.1230	0.2564(8)	0.2538(8)	0.4129(36)	0.2849(13)	0.3332(40)	0.3324(38)	0.3247(41)	0.3608(50)
0.1240	0.1235	0.2498(8)	0.2484(8)	0.4099(40)	0.2800(13)	0.3275(42)	0.3270(41)	0.3192(44)	0.3565(54)
0.1240	0.1240	0.2430(9)	–	0.4070(44)	0.2751(14)	0.3218(46)	–	0.3136(48)	0.3527(60)
0.1240	0.1245	0.2359(9)	0.2375(10)	0.4041(50)	0.2704(16)	0.3162(52)	0.3175(55)	0.3083(54)	0.3498(68)
0.1245	0.1230	0.2451(9)	0.2404(9)	0.4054(46)	0.2754(15)	0.3239(53)	0.3225(49)	0.3143(52)	0.3548(64)
0.1245	0.1235	0.2383(10)	0.2349(9)	0.4035(51)	0.2705(16)	0.3180(57)	0.3168(53)	0.3085(56)	0.3507(69)
0.1245	0.1240	0.2312(10)	0.2294(10)	0.4016(58)	0.2656(18)	0.3122(63)	0.3112(60)	0.3028(61)	0.3470(77)
0.1245	0.1245	0.2237(11)	–	0.4000(68)	0.2609(19)	0.3065(71)	–	0.2972(70)	0.3444(89)
fit range		28–56	28–56	16–24	28–58	26–44	26–44	26–44	26–44

TABLE VII: The same as Table V for $\beta = 6.10$.

κ_1	κ_2	Positive parity baryons				Negative parity baryons			
		$m_{oct}(\Sigma)$	$m_{oct}(\Lambda)$	m_{sing}	m_{dec}	$m_{oct}(\Sigma)$	$m_{oct}(\Lambda)$	m_{sing}	m_{dec}
0.1230	0.1230	0.2382(4)	–	0.3466(30)	0.2560(7)	0.2967(23)	–	0.2925(20)	0.3103(26)
0.1230	0.1235	0.2320(5)	0.2329(5)	0.3417(32)	0.2511(08)	0.2911(25)	0.2919(25)	0.2875(21)	0.3059(28)
0.1230	0.1240	0.2257(5)	0.2276(5)	0.3365(35)	0.2463(08)	0.2854(27)	0.2874(27)	0.2827(22)	0.3017(32)
0.1230	0.1245	0.2193(5)	0.2223(5)	0.3311(39)	0.2417(09)	0.2796(29)	0.2835(33)	0.2783(25)	0.2981(38)
0.1235	0.1230	0.2271(5)	0.2262(5)	0.3370(35)	0.2462(8)	0.2867(26)	0.2858(26)	0.2826(22)	0.3014(31)
0.1235	0.1235	0.2208(5)	–	0.3325(38)	0.2413(09)	0.2809(28)	–	0.2776(24)	0.2969(34)
0.1235	0.1240	0.2143(5)	0.2154(5)	0.3277(42)	0.2365(10)	0.2750(31)	0.2762(31)	0.2728(26)	0.2926(38)
0.1235	0.1245	0.2076(6)	0.2101(6)	0.3226(48)	0.2319(11)	0.2689(34)	0.2722(38)	0.2683(29)	0.2889(46)
0.1240	0.1230	0.2160(5)	0.2137(5)	0.3268(42)	0.2366(10)	0.2768(32)	0.2746(31)	0.2729(26)	0.2929(39)
0.1240	0.1235	0.2095(6)	0.2082(5)	0.3232(47)	0.2317(11)	0.2709(34)	0.2695(34)	0.2680(28)	0.2883(43)
0.1240	0.1240	0.2028(6)	–	0.3193(53)	0.2270(12)	0.2646(37)	–	0.2631(31)	0.2840(49)
0.1240	0.1245	0.1958(6)	0.1974(6)	0.3150(62)	0.2225(13)	0.2581(42)	0.2604(45)	0.2586(35)	0.2803(59)
0.1245	0.1230	0.2049(6)	0.2006(6)	0.3151(55)	0.2276(12)	0.2680(44)	0.2628(42)	0.2638(33)	0.2855(56)
0.1245	0.1235	0.1982(7)	0.1950(6)	0.3133(63)	0.2228(14)	0.2617(48)	0.2575(45)	0.2588(36)	0.2809(63)
0.1245	0.1240	0.1912(7)	0.1894(7)	0.3114(74)	0.2182(15)	0.2551(53)	0.2523(50)	0.2540(40)	0.2765(72)
0.1245	0.1245	0.1839(8)	–	0.3094(91)	0.2139(18)	0.2479(61)	–	0.2493(46)	0.2727(88)
fit range		40–64	40–64	24–36	44–64	36–52	36–52	32–52	36–52

parity baryon masses was evaluated as 5% by comparing the masses on lattices with volume sizes 1.5fm and 2.2fm (1.6fm and 2.1fm) at $\beta = 6.0$ (6.2) on quenched isotropic lattices. This amount of finite size effect may also exist in our results, while our lattice volumes are close to the larger ones in Ref. [6].

- *Lattice discretization error*

Table VIII shows the baryon masses on each lattice. We find it hard to take the continuum limit even for the ground state baryons and mesons, since only the three β 's are taken here and their behavior is not so smooth that one can apply a simple extrapolation. Although such fluctuating behavior of data

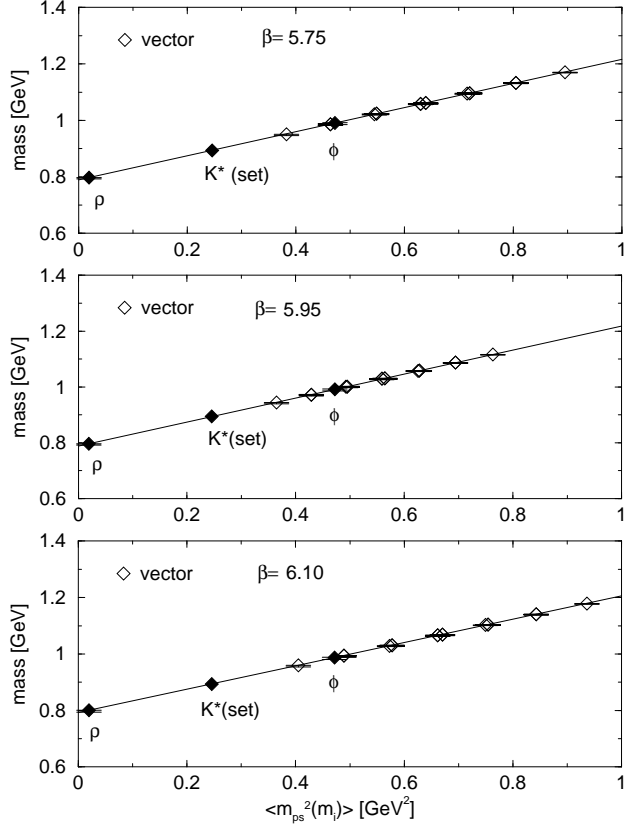


FIG. 2: Spectrum of the vector meson in the physical units.

may be largely due to the lack of statistics, genuine discretization errors would not also be negligible. In the range of lattice cutoff 1–2 GeV, the fluctuation of masses is at most about 5%, except for the case of Λ_{sing}^+ for which 7% deviation is found. This gives us a hint on the potential size of the discretization errors. We also note that Ref. [20] examined how the $O(\alpha a)$ and $O(a^2)$ discretization effects decrease as β increases in the meson sectors, and found that those in the calibration of γ_F are sufficiently reduced already at $\beta = 6.10$. For these reason we discuss physical consequences of our result mainly based on the data of $\beta = 6.10$ lattice in the next section.

- *Chiral extrapolation*

As stated in the previous subsection the non-analyticity in the chiral extrapolation of the nucleon at the quenched level are reported from the study of the chiral perturbation theory[25]. We have, however, taken the naive linear extrapolation for both the positive and negative parity baryons, because the results for the baryon masses seem to be well described with the linear relation, probably due to relatively large quark mass region adopted in this work. In addition, the behavior of the neg-

TABLE VIII: Hadron spectrum at physical quarks masses in the physical units.

	$\beta = 5.75$	$\beta = 5.95$	$\beta = 6.10$
ρ [GeV]	0.7973(52)	0.7965(53)	0.8005(65)
K^*	—	—	—
ϕ	0.9905(55)	0.9913(53)	0.9873(66)
N	1.1118(84)	1.0781(81)	1.1055(72)
Λ	1.2095(75)	1.1825(75)	1.2002(67)
Σ	1.2256(76)	1.1982(76)	1.2173(67)
Ξ	1.3393(71)	1.3183(75)	1.3291(67)
Δ	1.366(23)	1.342(16)	1.3685(17)
Σ^*	1.459(20)	1.440(14)	1.4586(15)
Ξ^*	1.552(17)	1.538(12)	1.5486(13)
Ω	1.645(15)	1.635(11)	1.6387(12)
$N^{(-)}$	1.686(79)	1.599(59)	1.618(57)
$\Sigma^{(-)}$	1.784(67)	1.705(49)	1.717(49)
$\Xi^{(-)}$	1.882(56)	1.810(40)	1.816(42)
$\Lambda_{oct}^{(-)}$	1.788(66)	1.703(48)	1.700(49)
$\Lambda_{sing}^{(-)}$	1.732(28)	1.646(49)	1.725(39)
$\Delta^{(-)}$	1.806(84)	1.877(73)	1.833(80)
$\Sigma^{*(-)}$	1.896(72)	1.955(61)	1.913(69)
$\Xi^{*(-)}$	1.986(60)	2.032(50)	1.994(57)
$\Omega^{(-)}$	2.077(49)	2.109(39)	2.074(46)
$\Lambda_{sing}^{(+)}$	2.288(58)	2.292(46)	2.150(70)

ative parity baryon masses near the chiral limit is less known. Therefore, it is difficult to estimate the non-analyticity in the chiral extrapolation from the present results. The quantitative estimate of its effect on the negative parity baryon masses is a future problem with high precision data with small quark masses.

- *Quenching effects*

There is about 10% uncertainty for the ground state hadron spectra coming from the quenching effect. Since we measure the negative parity baryons using the same correlators as the positive parity ones, it is natural to consider the error of the negative parity baryons as the same order. The size of quenching effect must be kept in mind particularly in comparison of the mass of $\Lambda(1405)$ with other baryons and with the experimental value, since our strategy to elucidate the nature of $\Lambda(1405)$ makes use of the virtue of the quenched calculation.

IV. DISCUSSION

Our numerical results for the hadrons spectra are shown in Fig. 3 and Table VIII. One sees that the masses of the negative parity baryons are heavier than those of the corresponding positive parity sectors, as expected.

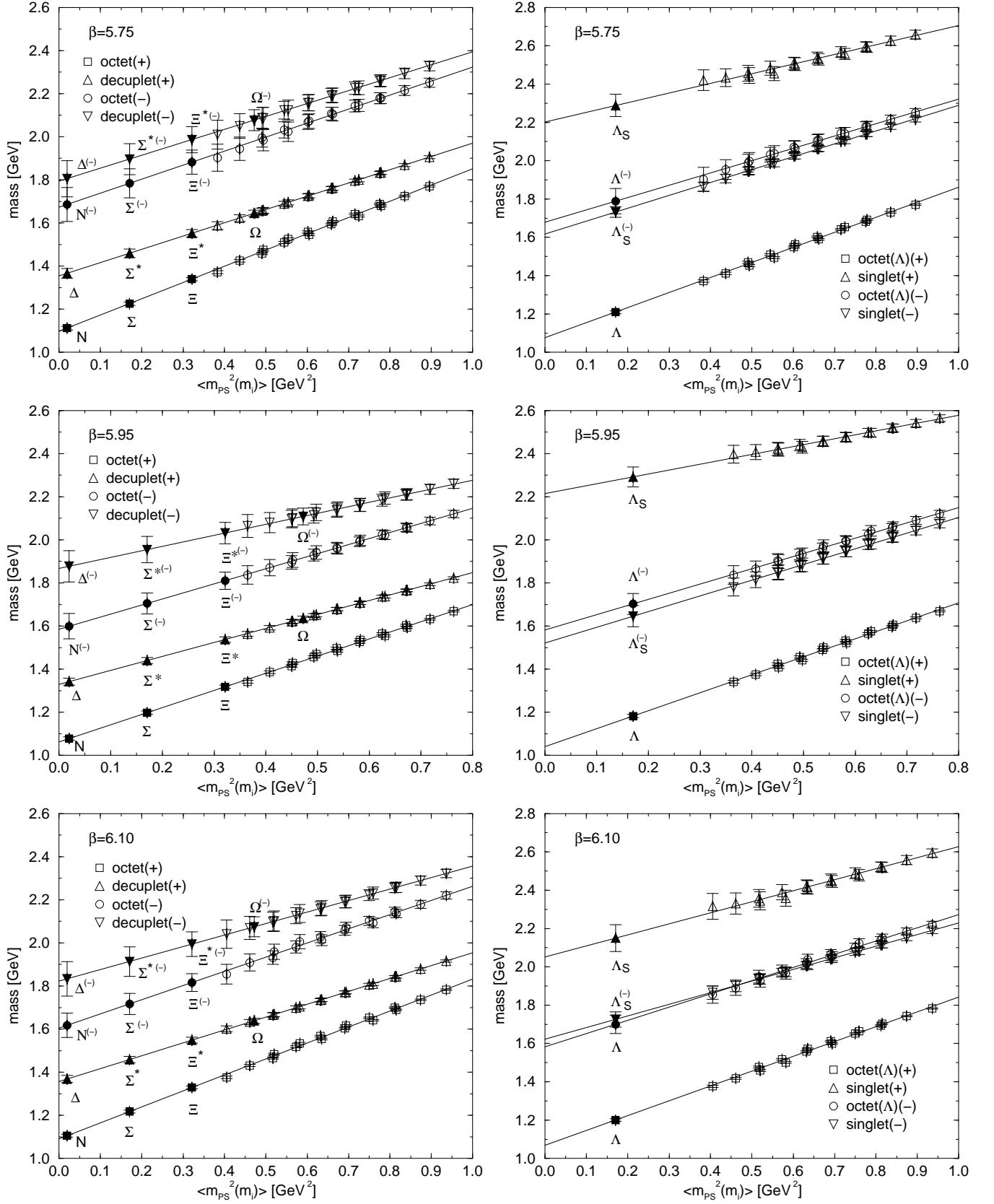


FIG. 3: The spectra of positive and negative parity baryons. For each β , the octet and the decuplet baryons are shown in the left panel and octet(Λ) and singlet baryons in the right panel. The horizontal axis denotes the averaged pseudoscalar mass square. The open symbols denote lattice data and the filled symbols the results for the physical quark masses determined via linear chiral extrapolation.

The flavor singlet baryon is, however, an exception: the positive parity baryon is much heavier than the negative parity one. It is consistent with the quark model, in which the flavor singlet positive parity baryon belongs to the 70-dimensional representation of the $SU(6)$ symmetry with the principal quantum number $N = 2$. This multiplet is in general heavier than that belonging to the negative parity baryons. QCD sum rule analysis[26] and the other recent lattice calculation [7] also predict the mass of the flavor singlet negative parity baryon lighter than that of the positive one.

In order to compare our lattice results with experimental values, various baryon masses at $\beta = 6.10$ together with the experimental values are shown in Fig. 4. For the positive parity baryons, the nucleon and the delta masses are somewhat higher than the experimental ones. As stated in the previous section, there exists the non-analyticity of the chiral extrapolation of the nucleon[25]. This effect lowers the nucleon mass in the chiral limit compared with the naive linear extrapolation, although we have not taken into account the non-analyticity due to the absence of the signal in our results. The other positive parity baryons with strangeness reproduce the experimentally observed masses within 10% deviations.

As for the negative parity baryons, most of the present lattice results comparatively well reproduces the experimental spectra, although they have a relatively large statistical error. However, there is one exceptional case: the lattice result of the flavor singlet negative parity baryon is much heavier than the experimentally observed $\Lambda(1405)$ with the difference of more than 300 MeV. We note that since the flavor singlet baryon has one strange quark, the ambiguity from the chiral extrapolation should be less than that of the nucleon and the delta. The difference between the lattice result and the experimental value of $\Lambda(1405)$ is, however, the largest of all. Even if we take the quenching effect of 10% level into account, this large discrepancy cannot be accepted. Therefore, the numerical result for the flavor singlet baryon is different feature from other channels, which indicates that it is much heavier than $\Lambda(1405)$. Thus, we conclude that the present lattice result indicates that the three valence quark picture fails to represent the experimentally observed $\Lambda(1405)$, i.e., the overlap with the 3Q component of $\Lambda(1405)$ is small. The other possible candidate for $\Lambda(1405)$ is a five-quark (5Q) $N\bar{K}$ state. There exists the QCD sum rule approach for the multi-quark correlation functions[27]. Lattice calculations of the 5Q state will also elucidate the nature of $\Lambda(1405)$.

We focus on other negative parity baryons. The mass ratio between the positive and negative sectors is shown in Table IX. One sees that the mass difference between two becomes smaller for both the octet and decuplet baryons as the quark mass increases, which is consistent with the physical values shown in the table. This behavior is also reported in another lattice QCD analysis by the domain wall fermion[5]. From Fig. 4 and Table IX, we see that the lattice results of the flavor octet and

decuplet sectors are all close to the observed lowest-lying negative parity baryons, $N(1535)$, $\Lambda(1670)$, $\Sigma(1620)$ and $\Delta(1700)$, in spite of the relatively large statistical error. The $\Sigma(1620)$, which is experimentally confirmed as the negative parity strange baryon with $J^P = 1/2^-$ [17], is consistent with the parity partner of the Σ baryon. The parity partner of the Ξ baryon is expected to be $\Xi(1690)$ from our calculation, although the spin-parity of $\Xi(1690)$ is not yet confirmed experimentally. For the decuplet baryons, we can regard the parity partner of $\Delta(1232)$ as $\Delta(1700)$, though the experimental data is poor. The positive parity singlet is much heavier than the negative parity decuplet, which makes it much difficult to investigate the flavor singlet baryons both theoretically and experimentally.

Finally we comment on recent lattice studies on the negative parity baryons. Sasaki et al. investigated the negative parity (non-strange) nucleon with the domain wall fermion[5]. Their lattice is $16^3 \times 32$ at $\beta = 6.0$ ($a^{-1} = 1.9$ GeV) and the result is $N^{(-)}/N^{(+)} \sim 1.45$, which is consistent with ours. Gökler et al. studied the negative parity (non-strange) nucleon using the $O(a)$ improved Wilson quark on the isotropic lattices with the sizes $16^3 \times 32$ to $32^3 \times 64$ [6]. They obtained the similar result, $N^{(-)}/N^{(+)} = 1.50(3)$. Melnitchouk et al. also studied the negative parity baryons using the $O(a)$ improved Wilson quark on the isotropic lattice, $16^3 \times 32$ ($a = 0.125$ fm)[7]. Since they did not carry out the chiral extrapolation we do not compare the results quantitatively, but the qualitative behavior is similar to us. They also investigated the flavor singlet baryons. Instead of the flavor singlet interpolating field, they used the “common” interpolating field which is the common part of the interpolating fields for the octet Λ hyperon and the singlet baryon. The result is much heavier than the experimental value of $\Lambda(1405)$ even for such an fields. Lee et al. investigated the excited state baryons with the overlap fermion with the lattice $16^3 \times 28$ [8]. They employed the curve-fitting method for the mass fitting and obtained the baryons masses lower than that from the conventional fitting method. Thus, their results seem to be lower than ours and the other’s, while they did not carry out the chiral extrapolation. Dynamical quark simulation of excited state baryons is also in progress [9]. As for the negative parity nucleon, their present result is consistent with the quenched result within statistical errors.

V. CONCLUSION

We have studied the mass spectra of the negative parity baryons and the flavor singlet baryons in the quenched anisotropic lattice QCD. We use three lattices of almost the same physical spatial volume, about 2 fm, with the spatial cutoffs $a_\sigma^{-1} = 1\text{--}2$ GeV and the renormalized anisotropy $\xi = a_\sigma/a_\tau = 4$. We adopt the standard Wilson plaquette gauge action and the $O(a)$ improved Wilson quark action at the tadpole-improved tree-level [20].

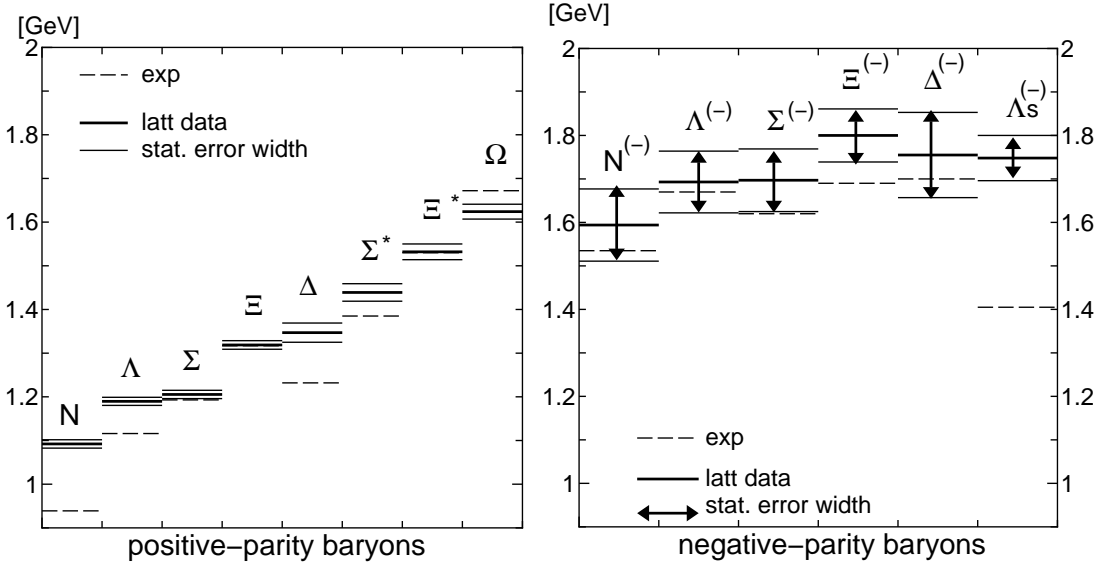


FIG. 4: Various baryon masses from the $\beta = 6.10$ lattice together with the masses of experimentally observed baryons. Experimental values of the negative parity baryons are taken to be $N(1535)$, $\Lambda(1670)$, $\Sigma(1620)$, $\Xi(1690)$, $\Delta(1700)$ and $\Lambda(1405)$ from left.

TABLE IX: The ratio of negative and positive parity baryon masses. In the last line, the ratio of flavor singlet negative parity and octet positive parity baryon masses is also listed. Physical values of the negative parity baryons are taken to be $N(1535)$, $\Sigma(1620)$, $\Xi(1690)$, $\Lambda_{oct}(1670)$, $\Lambda_{sing}(1405)$ and $\Delta(1700)$. (*)Note that the parity of $\Xi(1690)$ is not yet confirmed.

	$\beta = 5.75$	$\beta = 5.95$	$\beta = 6.10$	physical value
N	1.516(70)	1.484(54)	1.463(51)	1.635
Σ	1.456(54)	1.423(40)	1.410(40)	1.358
Ξ	1.405(41)	1.373(30)	1.366(31)	1.282*
Λ_{oct}	1.479(54)	1.440(40)	1.417(40)	1.496
Λ_{sing}	0.757(22)	0.718(26)	0.802(32)	
Δ	1.322(64)	1.399(55)	1.339(61)	1.380
Σ^*	1.299(52)	1.358(43)	1.312(49)	
Ξ^*	1.280(41)	1.321(33)	1.288(38)	
Ω	1.263(31)	1.290(24)	1.266(29)	
$m_{\Lambda_{sing}^{(-)}} / m_{\Lambda_{oct}^{(+)}}$	1.432(23)	1.392(42)	1.437(34)	1.259

The positive and negative parity baryon masses are extracted from the same baryon correlators based on the three valence quark picture.

Compared with the experimental values, our present results of the lattice calculation show that the flavor octet and decuplet negative parity baryons are all close to the lowest-lying negative parity baryons. We have also studied the negative parity baryons which are not found experimentally. For example the parity partner of the Ξ baryon is expected to be $\Xi(1690)$, whose spin-parity is not yet confirmed experimentally. The flavor decuplet negative parity baryons are also little known experimentally.

As for the flavor singlet baryons, the negative parity baryon is lighter than the positive one, as is con-

sistent with the quark models[10, 11], the QCD sum rule analysis[26] and other lattice simulations[7]. The present result of the mass of the negative parity flavor singlet baryon is much heavier than that of $\Lambda(1405)$, whose behavior is quite different from other negative parity baryons. Even considering the effect of the systematic errors, this discrepancy between the lattice result and experimental spectrum seems difficult to explain. This result implies that the three valence quark picture fails to represent the $\Lambda(1405)$ state, i.e., the overlap with the three-quark state of $\Lambda(1405)$ is small. For more definite understanding of $\Lambda(1405)$ spectrum, one needs more extensive work about the flavor singlet baryon such as the observation of the $N\bar{K}$ (five-quark) state. Such a study is interesting even at the quenched level, where

quark-antiquark pair creation (strictly speaking, dynamical quark loop effect) is absent and then the quark-level constitution of hadrons is definitely clear in the simulation.

From aspect of the chiral symmetry, the parity partner should be degenerate if the symmetry is restored at finite temperature and/or density. It is interesting to see how the mass difference between the parity partners changes at finite temperature on the lattice. Several works on it are already reported for the screening mass of the nucleon[28] and they favor the parity degeneracy at the chiral phase transition. Recently based on the chiral effective theory such as the linear sigma model[29] and the chiral perturbation theory[30], two different assignments for the negative parity baryons have been proposed: under the chiral transformation, the negative parity baryon transforms in the same way as the positive parity one in one scheme and in the opposite way in the other. These two assignments behave differently toward the chiral restoration. Therefore, it is interesting to study them

from the quark degrees of freedom such as in lattice QCD at finite temperature.

Acknowledgments

Y.N. thanks S. Sasaki, T. Blum and S. Ohta for useful discussions and comments. H.M. thanks T. Onogi and T. Umeda for useful discussions. The simulation was done on NEC SX-5 at Research Center for Nuclear Physics, Osaka University and Hitachi SR8000 at KEK (High Energy Accelerator Research Organization). H.M. is supported by Japan Society for the Promotion of Science for Young Scientists. Y.N. was supported by the center-of-excellence (COE) program at YITP, Kyoto University in most stage of this work and thanks RIKEN, Brookhaven National Laboratory and the U.S. Department of Energy for providing the facilities essential for the completion of this work.

-
- [1] CP-PACS Collaboration (S.Aoki et al.), Phys. Rev. Lett. **84**, 238 (2000).
 - [2] See for example for recent results, UKQCD collaboration, C.R. Alton et al., Phys. Rev. D **65**, 054502 (2002); JLQCD collaboration, T. Kaneko et al., *hep-lat/0209057*.
 - [3] N. Nakajima, H. Matsufuru, Y. Nemoto and H. Suganuma, proceedings of International Symposium on Hadrons and Nuclei, Seoul, Korea, AIP **CP594**, 349 (2001); H. Suganuma, N. Ishii, H. Matsufuru, Y. Nemoto and T.T. Takahashi, AIP **CP644**, 366 (2002).
 - [4] F. X. Lee and D.B. Leinweber, Nucl. Phys. B (Proc. Suppl.) **73**, 258 (1999).
 - [5] S. Sasaki, T. Blum and S. Ohta, Phys. Rev. D **65**, 074503 (2002).
 - [6] M. Göckeler, R. Horsley, D. Pleiter, P. E. L. Rakow, G. Schierholz, C. M. Maynard and D. G. Richards, Phys. Lett. B **532**, 63 (2002).
 - [7] W. Melnitchouk, S. Bilson-Thompson, F.D.R. Bonnet, F.X. Lee, D.B. Leinweber, A.G. Williams, J.M. Zanotti and J.B. Zhang, *hep-lat/0202022*.
 - [8] F.X. Lee, S.J. Dong, T. Draper, I. Horvath, K.F. Liu, N. Mathur and J.B. Zhang, *hep-lat/0208070*.
 - [9] UKQCD Collaboration, C.M. Maynard and LHP Collaboration, D.G. Richards, *hep-lat/0209165*.
 - [10] N. Isgur and G. Karl, Phys. Rev. D **20**, 1191 (1979).
 - [11] S. Capstick and N. Isgur, Phys. Rev. D **34**, 2809 (1986).
 - [12] For recent review, see e.g. S. Capstick and W. Roberts, *nucl-th/0008028*.
 - [13] T.T. Takahashi, H. Matsufuru, Y. Nemoto and H. Suganuma, Phys. Rev. Lett. **86**, 18 (2001); T.T. Takahashi, H. Suganuma, Y. Nemoto and H. Matsufuru, Phys. Rev. D **65**, 114509 (2002).
 - [14] G.S. Bali, Phys. Rept. **343**, 1 (2001).
 - [15] C. Alexandrou, Ph. de Forcrand and A. Tsapalis, Phys. Rev. D **65**, 054503 (2002).
 - [16] T.T. Takahashi and H. Suganuma, *hep-lat/0210024*.
 - [17] Particle Data Group, Phys. Rev. D **66**, 1 (2002).
 - [18] F. Karsch, Nucl. Phys. B **205**, 285 (1982).
 - [19] T. R. Klassen, Nucl. Phys. B **533**, 557 (1998).
 - [20] H. Matsufuru, T. Onogi and T. Umeda, Phys. Rev. D **64**, 114503 (2001); T. Umeda, H. Matsufuru and T. Onogi, Nucl. Phys. Proc. Suppl. **106**, 805 (2002).
 - [21] T. Umeda, R. Katayama, O. Miyamura and H. Matsufuru, Int. J. Mod. Phys. A **16**, 2215 (2001).
 - [22] J. Harada, A. S. Kronfeld, H. Matsufuru, N. Nakajima and T. Onogi, Phys. Rev. D **64**, 074501 (2001).
 - [23] A. X. El-Khadra, A. S. Kronfeld and P. B. Mackenzie, Phys. Rev. D **55**, 3933 (1997).
 - [24] G. P. Lepage and P. B. Mackenzie, Phys. Rev. D **48**, 2250 (1993).
 - [25] D.B. Leinweber, A.W. Thomas, K. Tsushima and S.V. Wright, Phys. Rev. D **66**, 094507, (2002); J.N. Labrenz and S.R. Sharpe, Phys. Rev. D **54**, 4595 (1996).
 - [26] D. Jido, N. Kodama and M. Oka, Phys. Rev. D **54**, 4532 (1996); D. Jido and M. Oka, *hep-ph/9611322*.
 - [27] J.P. Liu, Z. Phys. C **22**, 171 (1984); S. Choe, Eur. Phys. J. A **3**, 65 (1998); S. Choe, Eur. Phys. J. A **7**, 441 (2000).
 - [28] C. DeTar, J.B. Kogut, Phys. Rev. Lett. **59**, 399 (1987); Phys. Rev. D **36**, 2828 (1987); S. Gottlieb et al., Phys. Rev. Lett. **59**, 1881 (1987); A. Gocksch, P. Rossi and U.M. Heller, Phys. Lett. B **205**, 334 (1988); K. D. Born et al., Phys. Rev. Lett. **67**, 302 (1991); C. Bernard et al., Phys. Rev. D **45**, 3854 (1992); S. Gottlieb et al., Phys. Rev. D **47**, 3619 (1993); S. Gottlieb et al., Phys. Rev. D **55**, 6852 (1997).
 - [29] D. Jido, Y. Nemoto, M. Oka and A. Hosaka, Nucl. Phys. A **671**, 471 (2000); D. Jido, M. Oka and A. Hosaka, Prog. Theor. Phys. **106**, 873 (2001).
 - [30] Y. Nemoto, D. Jido, M. Oka and A. Hosaka, Phys. Rev. D **57**, 4124 (1998).